Monthly Notices of the ROYAL ASTRONOMICAL SOCIETY

MNRAS **510,** 4295–4301 (2022) https://doi.org/10.1093/mnras/stab3480
Advance Access publication 2021 December 1

Constraining the neutrino mass using a multitracer combination of two galaxy surveys and cosmic microwave background lensing

Mario Ballardini [1,2,3,4]★ and Roy Maartens[4,5,6]

[1]*Dipartimento di Fisica e Astronomia, Alma Mater Studiorum Università di Bologna, via Gobetti 93/2, I-40129 Bologna, Italy*
[2]*INAF/OAS Bologna, via Piero Gobetti 101, I-40129 Bologna, Italy*
[3]*INFN, Sezione di Bologna, via Irnerio 46, I-40126 Bologna, Italy*
[4]*Department of Physics & Astronomy, University of the Western Cape, Cape Town 7535, South Africa*
[5]*Institute of Cosmology & Gravitation, University of Portsmouth, Portsmouth PO1 3FX, UK*
[6]*National Institute of Theoretical & Computatiopnal Sciences (NITheCS), Pretoria 2600, South Africa*

Accepted 2021 November 26. Received 2021 November 26; in original form 2021 September 10

ABSTRACT

Measuring the total neutrino mass is one of the most exciting opportunities available with next-generation cosmological data sets. We study the possibility of detecting the total neutrino mass using large-scale clustering in 21 cm intensity mapping and photometric galaxy surveys, together with cosmic microwave background (CMB) information. We include the scale-dependent halo bias contribution due to the presence of massive neutrinos, and use a multitracer analysis in order to reduce cosmic variance. The multitracer combination of an SKAO-MID 21 cm intensity map with stage 4 CMB dramatically shrinks the uncertainty on total neutrino mass to $\sigma(M_\nu) \simeq 45$ meV, using only linear clustering information ($k_{\rm max} = 0.1\,h\,{\rm Mpc}^{-1}$) and without a prior on optical depth. When we add to the multitracer the clustering information expected from Legacy Survey of Space and Time, the forecast is $\sigma(M_\nu) \simeq 12$ meV.

Key words: neutrinos – cosmic background radiation – cosmological parameters – large-scale structure of Universe.

1 INTRODUCTION

Massive neutrinos leave unique imprints on cosmological observables throughout the history of the Universe (see Hannestad 2006; Lesgourgues & Pastor 2006, 2012; Wong 2011; Lattanzi & Gerbino 2018, for reviews). As a result, cosmology is likely to deliver the first experimental measurement of the total neutrino mass $M_\nu \equiv \sum m_\nu$.

Cosmological data from *Planck* 2018 (Planck Collaboration I 2020a; Planck Collaboration VIII 2020c) in combination with BOSS DR12 clustering information (BOSS Collaboration 2017), currently provide the constraint $M_\nu < 120$ meV at 95 per cent confidence level (CL, Vagnozzi et al. 2017; Ivanov, Simonović & Zaldarriaga 2020; Planck Collaboration VI 2020b). The current best neutrino mass limit is $M_\nu < 90$ meV (95 per cent CL) (Di Valentino, Gariazzo & Mena 2021), which uses also the additional information from Pantheon Type Ia supernovae and eBOSS DR16 cosmological measurements.

These limits are model dependent and usually weaken in cosmologies beyond the Lambda cold dark matter (ΛCDM) + M_ν model, in particular for cosmologies with extended dark energy models or modified theories of gravity (Vagnozzi et al. 2017; Ballardini et al. 2020; Roy Choudhury & Hannestad 2020; Sekiguchi & Takahashi 2021).

On the other hand, future cosmic microwave background (CMB) anisotropy observations from ground-based experiments and satellites, such as CMB-S4,[1] LiteBIRD,[2] and the Simons Observatory,[3] together with large-scale structure surveys that will be performed by DESI,[4] *Euclid*,[5] *Roman Space Telescope*,[6] Rubin Observatory,[7] SKA Observatory,[8] and others, promise a robust detection of the cosmological neutrino mass also for extended models (Allison et al. 2015; Villaescusa-Navarro, Bull & Viel 2015; Schmittfull & Seljak 2018; Yu et al. 2018; Boyle 2019; Brinckmann et al. 2019; Sprenger et al. 2019).

Neutrinos can travel cosmological distances during structure formation, modifying halo formation on large scales and inducing scale dependence of the halo bias around the neutrino free-streaming scale. This changes the relation between the halo number density and the matter (CDM + baryon) density contrast. The effect was predicted by Villaescusa-Navarro et al. (2014), Castorina et al. (2014), and LoVerde (2014), and measured in N-body simulations by Villaescusa-Navarro et al. (2014), Chiang et al. (2018), and Chiang, LoVerde & Villaescusa-Navarro (2019).

LoVerde (2016) proposed a very promising way to target the detection of the cosmological neutrino mass using the so-called

★ E-mail: mario.ballardini@inaf.it

[1]https://cmb-s4.org
[2]http://litebird.jp
[3]https://simonsobservatory.org
[4]https://www.desi.lbl.gov
[5]https://www.euclid-ec.org
[6]https://wfirst.gsfc.nasa.gov
[7]https://www.lsst.org
[8]https://www.skatelescope.org

multitracer approach (Seljak 2009) and focusing on this scale-dependent feature in the halo bias. Halo bias is particularly interesting because it is a quantity that is not subject to cosmic variance when combining the information coming from different tracers of large-scale structure.

While the importance of the scale-dependent bias due to massive neutrinos and its consequences for parameter inference has been investigated and stressed in Raccanelli, Verde & Villaescusa-Navarro (2019) and Vagnozzi et al. (2018), in our work we investigate the possibility to improve the neutrino mass measurement through the combination and cross-correlation of radio, optical, and microwave cosmological observations.

This paper is organized as follows: In Section 2, we briefly review the scale-dependent features imprinted on the halo bias in cosmologies with massive neutrinos. We summarize the key specifications for the radio [SKAO-MID band 1 and the futuristic PUMA 21 cm intensity mapping (IM)], optical (Legacy Survey of Space and Time; LSST), and microwave (CMB-S4) surveys considered in our analysis in Section 3. We discuss the cross-correlation coefficient between CMB lensing and large-scale structure clustering in Section 4. Finally, we present our results in Section 5 and we draw our conclusions in Section 6.

2 SCALE-DEPENDENT BIAS FROM MASSIVE NEUTRINOS

On very large scales, there is a linear relationship between fluctuations in the number density of haloes, $\delta_{\rm h} \equiv \delta n_{\rm h}/n_{\rm h}$, and fluctuations in the underlying density field, $\delta_X \equiv \delta\rho_X/\rho_X$ (LoVerde 2014):

$$\delta_{\rm h} = b\delta_X \,, \tag{1}$$

where X denotes baryons (b), CDM (c), massive neutrino (ν), or a combination of them.

On scales above the baryonic Jeans scale, baryons and CDM behave indistinguishably and can be treated as a single fluid, with energy density $\rho_{\rm bc} \equiv \rho_{\rm b} + \rho_{\rm c}$, and number density contrast

$$\delta_{\rm bc} = \frac{\Omega_{\rm b}\delta_{\rm b} + \Omega_{\rm c}\delta_{\rm c}}{\Omega_{\rm b} + \Omega_{\rm c}} \,. \tag{2}$$

The halo bias defined with respect to the CDM + baryon fluid,

$$b_{\rm bc} = \frac{\delta_{\rm h}}{\delta_{\rm bc}} \,, \tag{3}$$

is scale independent on large scales and universal, since halo formation is governed by local processes only (Kaiser 1984; Bardeen et al. 1986; Coles 1993; Mann, Peacock & Heavens 1998). Scale-dependent features might arise due to properties inherited in galaxy formation and evolution, and they naturally appear on small scales (Castorina et al. 2014).

If we define the halo bias relative to the total matter field

$$b_{\rm m} = \frac{\delta_{\rm h}}{\delta_{\rm m}} \,, \tag{4}$$

where

$$\delta_{\rm m} = \frac{\Omega_{\rm bc}\delta_{\rm bc} + \Omega_\nu\delta_\nu}{\Omega_{\rm m}} = (1 - f_\nu)\delta_{\rm bc} + f_\nu\delta_\nu \,, \tag{5}$$

then this manifests a scale-dependent feature from massive neutrinos, with a step-like behaviour, around the neutrino free-streaming scale (Eisenstein & Hu 1997; Hu & Eisenstein 1998; Castorina et al. 2014; LoVerde 2014; Villaescusa-Navarro et al. 2014). This is illustrated in Fig. 1.

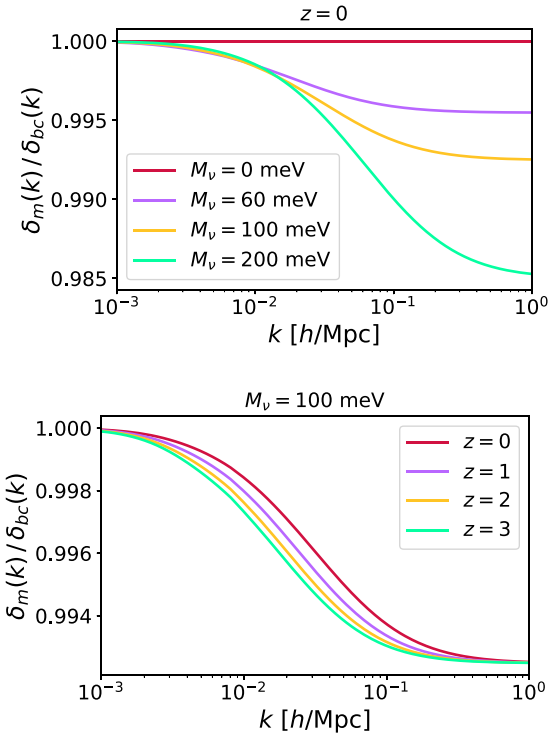

Figure 1. Scale-dependence induced in the matter density contrast in the presence of a single massive neutrino. Top panel: At $z = 0$, with $M_\nu = 0$, 60, 100, and 200 meV. Bottom panel: With $M_\nu = 100$ meV, at $z = 0$, 1, 2, and 3.

On scales larger than the neutrino free-streaming scale, and when neutrinos are non-relativistic, the bc and ν fluids are tightly coupled, $\delta_{\rm bc} \approx \delta_\nu$, leading to $\delta_{\rm m} \approx \delta_{\rm bc}$. On smaller scales, neutrino perturbations are damped and neutrinos do not cluster, so that $\delta_{\rm m} \approx (1 - f_\nu)\delta_{\rm bc}$. The amplitude of the feature is larger in cosmologies with larger neutrino masses (see Fig. 1), and for more massive haloes (LoVerde 2014; Raccanelli et al. 2019).

3 METHODOLOGY AND SIMULATED DATE SETS

Following Ballardini, Matthewson & Maartens (2019), we use the Fisher matrix formalism to forecast constraints on the cosmological parameters, assuming that the observed fields are Gaussian random distributed.

The Fisher matrix at the power spectrum level is then

$$F_{\alpha\beta} = f_{\rm sky} \sum_{\ell=\ell_{\rm min}}^{\ell_{\rm max}} \left(\frac{2\ell+1}{2}\right) {\rm tr}\left[\boldsymbol{C}_{\ell,\alpha}\, \boldsymbol{\Gamma}_\ell^{-1}\, \boldsymbol{C}_{\ell,\beta}\, \boldsymbol{\Gamma}_\ell^{-1}\right] , \tag{6}$$

where $\boldsymbol{C}_\ell = [C_\ell(z_i, z_j)]$ is the covariance matrix, $\boldsymbol{C}_{\ell,\alpha} = \partial\boldsymbol{C}_\ell/\partial\theta_\alpha$ is its derivative with respect to the cosmological parameter θ_α, and $\boldsymbol{\Gamma}_\ell = \boldsymbol{C}_\ell + \boldsymbol{\mathcal{N}}_\ell$ is the observed covariance, with $\boldsymbol{\mathcal{N}}_\ell$ the diagonal noise matrix. This equation assumes that all experiments observe the same patch of sky, with the same $f_{\rm sky}$.

We consider for each experiment its own sky fraction, while for the cross-correlations we use the estimated overlapping sky fractions. In particular, we assume $f_{\rm sky} = 0.4$ for CMB-S4, $f_{\rm sky} \simeq 0.48$ for SKAO-MID, $f_{\rm sky} = 0.5$ for PUMA, $f_{\rm sky} \simeq 0.33$ for LSST, and $f_{\rm sky} = 0.4$ for CMB-S4 × SKAO-MID, $f_{\rm sky} = 0.4$ for CMB-S4 × PUMA, $f_{\rm sky} \simeq 0.33$ for CMB-S4 × LSST, $f_{\rm sky} \simeq 0.33$ for SKAO-MID × LSST,

and $f_{\rm sky} \simeq 0.33$ for PUMA × LSST. We calculate the Fisher matrices over the common patch and then we add them together.

The angular power spectra are

$$C_\ell^{XY}(z_i,\, z_j) = 4\pi \int \frac{{\rm d}k}{k}\, \mathcal{P}_\mathcal{R}(k)\, I_\ell^X(k,\, z_i)\, I_\ell^Y(k,\, z_j)\,. \tag{7}$$

Here $X,\ Y = {\rm T}, {\rm E}, \phi$ for the CMB, and $= \Delta_{\rm g}$ or $\Delta_{\rm H\,I}$ for the galaxy or IM surveys of post-reionization neutral hydrogen (H I), where $\Delta_{\rm g} = \delta_{\rm g} +$ observational corrections from observing on the past light-cone, and similarly for $\Delta_{\rm H\,I}$ (see Challinor & Lewis 2011; Alonso & Ferreira 2015; Alonso et al. 2015; Fonseca et al. 2015; Ballardini & Maartens 2019; Ballardini et al. 2019, for details). $\mathcal{P}_\mathcal{R}$ is the dimensionless primordial power spectrum and the large-scale structure kernels are

$$I_\ell^{\Delta_{\rm g}}(k,\, z_i) = \int {\rm d}z\, n_{\rm g}^i(z)\, \Delta_\ell^g(k,\, z)\,, \tag{8}$$

$$I_\ell^{\Delta_{\rm H\,I}}(k,\, z_i) = \int {\rm d}z\, W_{\rm th}(z,\, z_i)\, \bar{T}_{\rm H\,I}(z)\, \Delta_\ell^{\rm H\,I}(k,\, z)\,, \tag{9}$$

where $\Delta_\ell^g, \Delta_\ell^{\rm H\,I}$ are the angular transfer functions (Ballardini & Maartens 2019), and $W_{\rm th}(z,\, z_i)$ is a smoothed top-hat window function for the i-th bin to ensure numerical stability. $n_{\rm g}(z_i)$ includes a Gaussian window over the average angular number density $\bar{n}_{\rm g}$ (see below), and $\bar{T}_{\rm H\,I}$ is the average brightness temperature. We refer the reader to Hu & White (1997) for the details of the CMB temperature and polarization window functions.

The standard cosmological parameter vector that we use is

$$\boldsymbol{\theta} = \left\{\omega_{\rm b},\, \omega_{\rm c},\, H_0,\, \tau,\, \ln\left(10^{10} A_{\rm s}\right),\, n_{\rm s},\, M_\nu\right\}. \tag{10}$$

We also include a pair of nuisance parameters for each redshift bin, in each of the large-scale structure surveys, allowing for a free redshift evolution of the clustering bias $b_{\rm g}$, or of the combination $\bar{T}_{\rm H\,I} b_{\rm H\,I}$ for IM, and for a free redshift evolution of the galaxy magnification bias $s_{\rm g}$.

The fiducial cosmology used for the standard cosmological parameters follows *Planck* 2018 (Planck Collaboration VI 2020b): $\omega_{\rm b} = 0.022383$, $\omega_{\rm c} = 0.12011$, $H_0 = 67.32\ {\rm km\,s^{-1}\,Mpc^{-1}}$, $\tau = 0.0543$, $\ln(10^{10} A_{\rm s}) = 3.0448$, $n_{\rm s} = 0.96605$, and $M_\nu = 60$ meV. We assume one massive and two massless neutrinos with $N_{\rm eff} = 2.046$. All angular power spectra are calculated using a modified version of the publicly available code[9] `CAMB` (Lewis, Challinor & Lasenby 2000; Challinor & Lewis 2011; Howlett et al. 2012). Small-scale non-linear corrections to the matter power spectrum are modelled with the `Halofit` model (Bird, Viel & Haehnelt 2012; Takahashi et al. 2012).

3.1 Radio survey: single-dish mode

We consider intensity maps of the 21 cm emission of neutral hydrogen. For the fiducial linear bias model and background H I brightness temperature, we use the fitting formulas (MeerKLASS Collaboration 2017):

$$b_{\rm H\,I}(z) = 0.667 + 0.178\, z + 0.0502\, z^2\,, \tag{11}$$

$$\bar{T}_{\rm H\,I}(z) = 0.0559 + 0.232\, z - 0.0241\, z^2\ {\rm mK}\,. \tag{12}$$

The noise variance for IM with $N_{\rm dish}$ dishes in single-dish mode in the frequency i-channel, assuming scale independence and no correlation between the noise in different frequency channels, is (Knox 1995; Bull et al. 2015; Durrer et al. 2020; Jolicoeur et al. 2021)

$$\sigma_{\rm H\,I}(\nu_i) = \frac{4\pi f_{\rm sky}\, T_{\rm sys}^2(\nu_i)}{2 N_{\rm dish}\, t_{\rm tot}\, \Delta\nu}\,, \tag{13}$$

$$T_{\rm sys}(\nu_i) = 25 + 60 \left(\frac{300\ {\rm MHz}}{\nu_i}\right)^{2.55}\ {\rm K}\,, \tag{14}$$

where $t_{\rm tot}$ is the total observing time. We assume the noise is deconvolved with a Gaussian beam, modelled as

$$\mathcal{N}_\ell^{\rm H\,I}(\nu_i) = \sigma_{\rm H\,I}(\nu_i)\, B_\ell^{-2}(\nu_i)\,, \tag{15}$$

with

$$B_\ell = \exp\left[-\ell(\ell+1)\frac{\theta_{\rm FWHM}^2}{16\ln 2}\right], \tag{16}$$

and

$$\theta_{\rm FWHM} = \frac{1.22\,\lambda_i}{D_{\rm dish}} \quad \text{where} \quad \lambda_i = \lambda_{21}(1+z_i)\,. \tag{17}$$

For the next-generation SKAO-MID, we follow the SKAO Cosmology Red Book (SKA Collaboration 2020) and use $N_{\rm dish} = 197$, $D_{\rm dish} = 15$ m, $t_{\rm tot} = 10^4$ h, observing over 20 000 deg^2 in the redshift range $0.35 \le z \le 3.05$ ($1050 \ge \nu \ge 350$ MHz, band 1). We divide the redshift range into 27 tomographic bins with width 0.1. The cleaning of foregrounds from the H I intensity map effectively removes the largest scales, $\ell \lesssim 5$ (Cunnington et al. 2019; Witzemann et al. 2019) and we take $\ell_{\rm min} = 5$.

3.2 Radio survey: interferometer mode

For interferometer-mode IM, the noise is (Bull et al. 2015; Alonso et al. 2017; Cosmic Visions 21 cm Collaboration 2018; Durrer et al. 2020; Jolicoeur et al. 2021)

$$\mathcal{N}_\ell^{\rm H\,I}(\nu_i) = \frac{4\pi f_{\rm sky}\, T_{\rm sys}^2(\nu_i)}{2 N_{\rm dish}\, t_{\rm tot}\, \Delta\nu}\, \frac{\theta_{\rm FWHM}^2(\lambda_i)}{\eta^2\, N_{\rm b}\, (\ell\lambda_i/(2\pi))\, \lambda_i^2}\,, \tag{18}$$

$$T_{\rm sys}(\nu_i) = \widetilde{T}_{\rm ampl} + \widetilde{T}_{\rm ground} + T_{\rm sky}\,, \tag{19}$$

where $\eta = 0.7$ is the aperture-efficiency factor, $N_{\rm b}$ is the density of baselines in the image plane, $\widetilde{T}_{\rm ampl} = 61.73$ K is the amplifier noise temperature corrected by the optical efficiency, $\widetilde{T}_{\rm ground} = 33.33$ K is due to the fraction of primary beam hitting the ground, and

$$T_{\rm sky}(\nu_i) = 2.7 + 25 \left(\frac{400\ {\rm MHz}}{\nu_i}\right)^{2.75}\ {\rm K}\,. \tag{20}$$

For the futuristic PUMA experiment, we follow Cosmic Visions 21 cm Collaboration (2018), PUMA Collaboration (2019) and assume $N_{\rm dish} = 32\,000$ dishes arranged in hexagonal close-packed array with 50 per cent fill factor, $D_{\rm dish} = 6$ m, an integration time of $t_{\rm tot} = 4 \times 10^4$ h, observing over half of the sky ($f_{\rm sky} = 0.5$) in the redshift range $0.3 \le z \le 6$. We divide the redshift range into 57 tomographic bins with width 0.1. As for SKAO, we take $\ell_{\rm min} = 5$.

3.3 Optical survey

For a next-generation photometric galaxy survey similar to the Vera C. Rubin Observatory's LSST, we assume a redshift distribution of sources of the form

$$\bar{n}_{\rm g}(z) \propto z^\alpha \exp\left[-\left(\frac{z}{z_0}\right)^\beta\right]\ {\rm gal\,arcmin^{-2}}\,. \tag{21}$$

[9] https://github.com/cmbant/CAMB

The distribution of sources in the i-th redshift bin, including photometric uncertainties, following Ma, Hu & Huterer (2005), is

$$n_{\rm g}^i(z) = \int_{z_{\rm ph}^i}^{z_{\rm ph}^{i+1}} {\rm d}z_{\rm ph}\, \bar{n}_{\rm g}(z)\, p(z_{\rm ph}|z)\,, \tag{22}$$

where we adopt a Gaussian distribution for the probability distribution of photometric redshift estimates $z_{\rm ph}$, given true redshifts z:

$$p(z_{\rm ph}|z) = \frac{1}{\sqrt{2\pi}\,\sigma_z} \exp\left[-\frac{\left(z-z_{\rm ph}\right)^2}{2\sigma_z^2}\right]. \tag{23}$$

The shot noise for galaxies in the i-th redshift bin is the inverse of the angular number density of galaxies:

$$\mathcal{N}_\ell^{{\rm g}i} = \left(\int {\rm d}z\; n_{\rm g}^i(z)\right)^{-1}. \tag{24}$$

For LSST clustering measurements, we assume a total number density of galaxies of $\bar{n}_{\rm g} = 48$ sources per arcmin^2, observed over 13 800 deg^2 and distributed in redshift according to (21), with $\alpha = 2$, $\beta = 0.9$, and $z_0 = 0.28$, corresponding to the Y10 gold sample ($i_{\rm lim} = 25.3$) specifications from LSST Dark Energy Science Collaboration (2018). We assume 10 tomographic bins spaced by 0.1, in the range $0.2 \le z \le 1.2$, with photometric redshift uncertainties $\sigma_z = 0.03\,(1+z)$. The fiducial model for the bias is $b_{\rm g}(z) = 0.95/D(z)$, where D is the growth factor (LSST Dark Energy Science Collaboration 2018). We impose $\ell_{\rm min} = 20$.

3.4 Microwave survey

We work with a possible CMB-S4 configuration assuming a 3 arcmin beam and $\sigma_{\rm T}^{1/2} = \sigma_{\rm P}^{1/2}/\sqrt{2} = 1\,\mu$K arcmin noise (CMB-S4 Collaboration 2016). We assume $\ell_{\rm min} = 30$ and a different cut at high ℓ of $\ell_{\rm max}^{\rm T} = 3000$ in temperature and $\ell_{\rm max}^{\rm P} = 5000$ in polarization, with $f_{\rm sky} = 0.4$.

For CMB temperature and polarization angular power spectra, the instrumental noise deconvolved with the instrumental beam is defined by (Knox 1995):

$$\mathcal{N}_\ell^{\rm T,P} = \sigma_{\rm T,P}\, B_\ell^{-2}\,, \tag{25}$$

where the Gaussian beam is given by (16).

For CMB lensing, we assume that the lensing reconstruction can be performed with the minimum variance quadratic estimator on the full sky, combining the TT, EE, BB, TE, TB, and EB estimators, calculated according to Hu & Okamoto (2002) with `quicklens`[10] and applying iterative lensing reconstruction (Hirata & Seljak 2003; Smith et al. 2012). We use the CMB-S4 lensing information in the range $30 \le \ell \le 3000$.

We will refer to the full set of CMB information including temperature, E-mode polarization, CMB lensing, and their cross-correlations, as simply 'CMB'.

4 CORRELATION BETWEEN CMB LENSING AND LARGE-SCALE STRUCTURE

The performance of the cross-correlation analysis depends on the cross-correlation coefficient. This is similar to the signal-to-noise ratio in each redshift bin (Ballardini & Maartens 2019), but without taking into account the number of modes and the sky fraction:

$$r_\ell^{X\phi}(z_i) = \frac{\left|C_\ell^{X\phi}(z_i)\right|}{\left[\Gamma_\ell^{XX}(z_i)\,\Gamma_\ell^{\phi\phi}\right]^{1/2}}\,, \tag{26}$$

where $X =$ H I or g. Fig. 2 shows the correlation coefficient of SKAO-MID, PUMA, and LSST redshift bins with CMB lensing expected from CMB-S4. The grey shading for $\ell < 30$ is the region where we do not have cross-correlation with CMB-S4.

The cross-correlation reaches a maximum at low redshift and it drops on small scales. Moving toward higher redshift, the correlation peaks at higher multipoles. This is connected to the position of the peak of the matter power spectrum in Fourier space at $k_{\rm peak} \sim 0.02\,h\,{\rm Mpc}^{-1}$, which is mapped to higher multipoles for higher redshift according to $\ell_{\rm peak}(z) \simeq k_{\rm peak}\,\chi(z)$ where $\chi(z)$ is the comoving radial distance.

The correlation coefficient and in particular the one obtained combining the tomographic redshift bins (black line in Fig. 2) can be maximized by optimizing the size and edges of the redshift bins. Choosing these weights such that they maximize the correlation coefficient between the joint analyses can be used to maximize the effect of sample variance cancellation.

Combining together the information from all redshift bins for each multipole, we can define the correlation coefficient (Sherwin & Schmittfull 2015)

$$r_\ell^{X\phi} = \left\{\sum_{i,j} r_\ell^{X\phi}(z_i)\left[r_\ell^{XX}\right]^{-1}(z_i,z_j)\,r_\ell^{X\phi}(z_j)\right\}^{1/2}, \tag{27}$$

where

$$r_\ell^{XX}(z_i,z_j) = \frac{C_\ell^{XX})(z_i,z_j)}{\Gamma_\ell^{XX}(z_i,z_j)}. \tag{28}$$

The combined cross-correlation coefficient for SKAO-MID and PUMA is higher (~ 90 per cent at $\ell \sim 50$) in the region of interest compared to LSST. This is due to the wider redshift range probed by the IM surveys compared to photometric surveys. Note that the cross-correlation coefficient for SKAO-MID drops at $\ell \sim 200$ because of the telescope beam (16).

5 RESULTS

We present in this section the uncertainties on the total neutrino mass M_ν for different combinations of cosmological surveys and considering a conservative $k_{\rm max} = 0.1\,h\,{\rm Mpc}^{-1}$, so that we consider on scales where linear perturbation theory is reliable. (Note that for SKAO-MID, the telescope beam effectively removes scales $k > 0.1\,h\,{\rm Mpc}^{-1}$). This k-cut is propagated to angular modes through the relation $\ell(z) \sim k\chi(z)$.

Note that CMB-S4 with $\ell_{\rm min} = 30$ delivers $\sigma(M_\nu) \simeq 115$ meV while complementing the low ℓ down to $\ell_{\rm min} = 2$ with LiteBIRD, it can reach $\sigma\,(M_\nu) \simeq 38$ meV.

Uncertainties are marginalized over all six standard cosmological parameters in (10). We also marginalize over the nuisance parameters that allow for a free redshift evolution of the clustering bias $b_{\rm g}$, or of the combination $T_{\rm H\,I} b_{\rm H\,I}$ for IM, and the magnification bias $s_{\rm g}$, for each redshift bin. This leads to 27 temperature-bias parameters for SKAO-MID, 57 temperature-bias parameters for PUMA, 10 clustering bias parameters, and 10 magnification bias parameters for the LSST survey.

[10] https://github.com/dhanson/quicklens

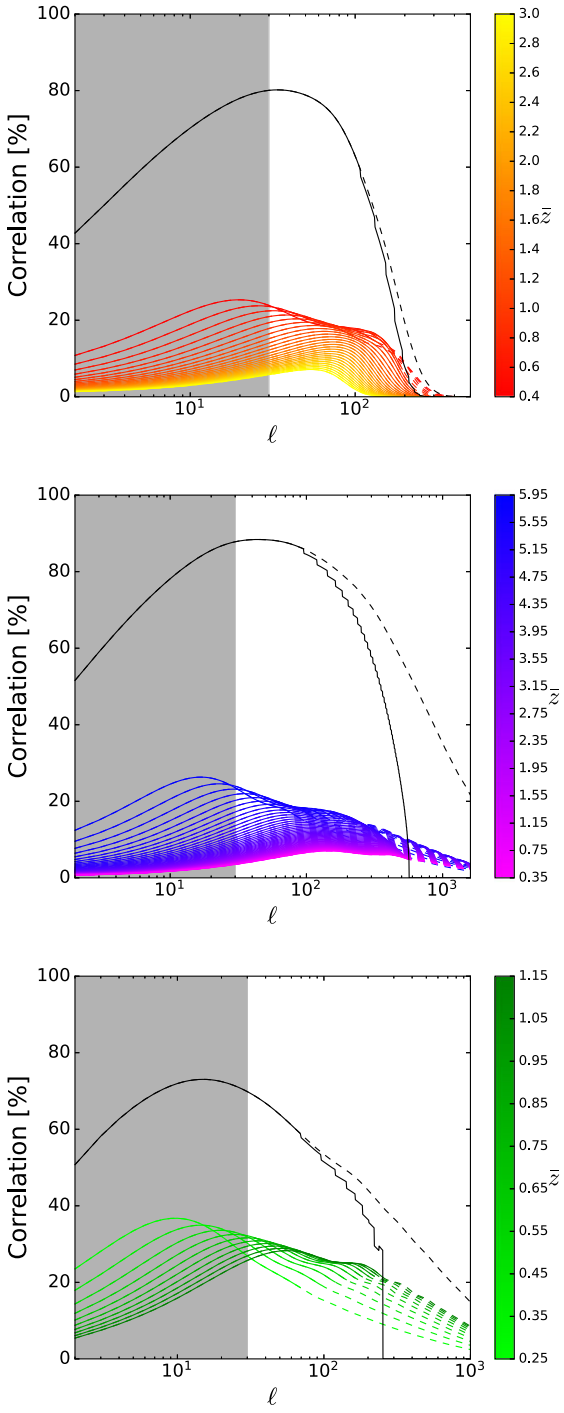

Figure 2. Expected correlation coefficient (26) between CMB-S4 lensing and SKAO-MID redshift bins (top panel), PUMA redshift bins (centre panel), and LSST photometric redshift bins (bottom panel). Black line shows the combined coefficient. Dashed lines denote the correlation coefficient calculated without imposing the cut of non-linear scales corresponding to $\ell(z) \sim 0.1\, h\chi(z)$.

The uncertainties for the single surveys with SKAO-MID, PUMA, and LSST are large compared to the fiducial assumption of $M_\nu = 60$ meV, as shown in Table 1. Single-tracer results do improve when the scale-dependent bias is included, but the major improvement comes from the multitracer. Including CMB information from CMB-S4

Table 1. Two-tracer case. Marginalized uncertainties on M_ν at 68 per cent CL including (right-hand column) or neglecting (left-hand column) the scale-dependent halo bias induced by massive neutrinos. Uncertainties are for $k_{\rm max} = 0.1\, h\,{\rm Mpc}^{-1}$.

	$\sigma(M_\nu)$ (meV)	
	Without bias	With bias
SKAO-MID	266	234
PUMA	76	77
LSST	846	782
SKAO-MID × CMB-S4	47	45
PUMA × CMB-S4	30	26
LSST × CMB-S4	69	62
SKAO-MID × LSST	240	118
PUMA × LSST	59	54

Table 2. As in Table 1, for the three-tracer case.

	$\sigma(M_\nu)$ (meV)	
	Without bias	With bias
SKAO-MID × LSST + CMB-S4	73	63
SKAO-MID × LSST × CMB-S4	17	12
PUMA × LSST + CMB-S4	28	28
PUMA × LSST × CMB-S4	12	11

with $\ell_{\rm min} = 30$, using the multitracer, delivers

$$\sigma\,(M_\nu) \simeq \begin{cases} 45\ {\rm meV} & {\rm SKAO\text{-}MID} \times {\rm CMB\text{-}S4}\,, \\ 26\ {\rm meV} & {\rm PUMA} \times {\rm CMB\text{-}S4}\,, \\ 62\ {\rm meV} & {\rm LSST} \times {\rm CMB\text{-}S4}\,, \end{cases} \tag{29}$$

for $k_{\rm max} = 0.1\, h\,{\rm Mpc}^{-1}$, while the combination of IM and LSST leads to

$$\sigma\,(M_\nu) \simeq \begin{cases} 118\ {\rm meV} & {\rm SKAO\text{-}MID} \times {\rm LSST}\,, \\ 54\ {\rm meV} & {\rm PUMA} \times {\rm LSST}\,. \end{cases} \tag{30}$$

When all three tracers are combined, the tightest constraints obtained are

$$\sigma\,(M_\nu) \simeq \begin{cases} 12\ {\rm meV} & {\rm SKAO\text{-}MID} \times {\rm LSST} \times {\rm CMB\text{-}S4}\,, \\ 11\ {\rm meV} & {\rm PUMA} \times {\rm LSST} \times {\rm CMB\text{-}S4}\,, \end{cases} \tag{31}$$

for $k_{\rm max} = 0.1\, h\,{\rm Mpc}^{-1}$.

We present the three-tracer case in Table 2. Adding CMB-S4 information to the multitracer combination of SKAO-MID and LSST reduces the error by a factor ∼2, to 63 meV. However, if we include all cross-correlations – between the CMB fields, IM, and number counts – then the error is reduced by a factor ∼5, to 12 meV. This effect is completely due to the cross-correlation with the CMB lensing ϕ: Neglecting the cross-correlation with E and T, we found the change in the uncertainties on the neutrino mass to be less than 1 per cent in all cases. Fig. 3 shows the marginalized uncertainties on the 3-dimensional ($\Omega_{\rm m,0}$, H_0, M_ν) parameter space.

As already shown in Brinckmann et al. (2019) and Yu et al. (2018), the addition of extra constraints on the optical depth $\tau_{\rm reio}$ at recombination can reduce further the uncertainties on the neutrino mass, breaking the partial degeneracy between M_ν and the normalization of the anisotropy $A_{\rm s}\exp(-2\tau_{\rm reio})$. We present in Table 3 the uncertainties on M_ν obtained when adding a Gaussian prior of $\sigma(\tau_{\rm reio}) = 0.008$, corresponding to current constraints from *Planck* (Planck Collaboration VI 2020b). We also consider $\sigma(\tau_{\rm reio}) = 0.001$, which is possible with future CMB cosmic-variance polarization experiments, or using independent information from 21 cm IM (Liu et al. 2016).

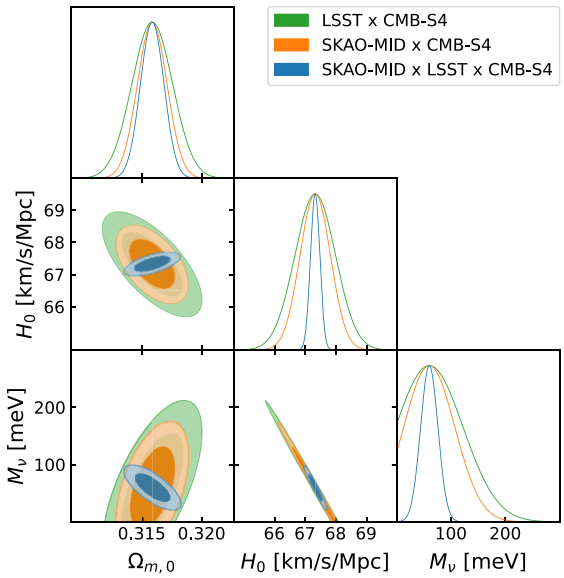

Figure 3. Marginalized 2-dimensional contours (68 per cent and 95 per cent CL) for $\Omega_{m,0}$, H_0, and M_ν. The multitracer combinations are: LSST x CMB-S4 (green), SKAO-MID × CMB-S4 (orange), and SKAO × LSST x CMB-S4 (blue).

Table 3. As in Table 2, including the scale-dependent halo bias in combination with a Gaussian prior on $\tau_{\rm reio}$.

	$\sigma(M_\nu)$ (meV)	
$\sigma(\tau_{\rm reio})$	0.008	0.001
SKAO-MID × LSST × CMB-S4	14	11
PUMA × LSST × CMB-S4	11	9

Note that considering our agnostic assumption about bias parameters any additional information regarding the clustering bias would improve the constraints on the neutrino mass. By contrast, marginalization over magnification bias does not significantly affect uncertainties on neutrino mass.

Finally, we find that modelling the scale-dependent features in the clustering bias due to the presence of massive neutrinos reduces the uncertainties significantly for the single-tracer cases, but for the multitracer cases there is only a slight improvement for such a small choice of $M_\nu = 60$ meV.

6 CONCLUSIONS

We presented Fisher forecast constraints on the total neutrino mass from upcoming 21 cm IM and photometric galaxy surveys, together with CMB lensing, temperature, and polarization data. We included the scale-dependent clustering bias that is induced by neutrinos. The critical feature of our analysis was to use a multitracer analysis that combined all the information, leading to significant improvements over single-tracer constraints or the simple addition of separate Fisher information for single tracers. The best results are achieved with a three-tracer combination of 21 cm IM, photometric survey, and CMB.

Constraints on the neutrino mass have been extensively studied; see e.g. Hall & Challinor (2012), Allison et al. (2015), Villaescusa-Navarro et al. (2015), Schmittfull & Seljak (2018), Brinckmann et al. (2019), Yu et al. (2018), Boyle (2019), Archidiacono, Hannestad & Lesgourgues (2020), Xu et al. (2021), Tanidis & Camera (2021), Bermejo-Climent et al. (2021), Sailer et al. (2021), and Bayer, Banerjee & Seljak (2021). While the combination of CMB and large-scale structure measurements is very powerful in breaking the geometrical degeneracy at background level, cosmological constraints depend strongly on the CMB low-ℓ measurements. Uncertainties of $\sigma(M_\nu) \simeq 20$–30 meV, corresponding to a 2σ–3σ detection for a minimum neutrino mass $M_\nu = 60$ meV, have been forecast when combining CMB anisotropies and future survey number counts, and including the *Planck* constraint $\sigma(\tau_{\rm reio}) \simeq 0.008$ on reionization (Planck Collaboration VI 2020b). These uncertainties are robust for extensions of the ΛCDM concordance model, such as cosmologies where also $N_{\rm eff}$ and the dark energy parameters are varied (Boyle 2019; Brinckmann et al. 2019). Moreover, the combination of different late-time probes such as baryon acoustic oscillations, galaxy clustering, galaxy weak lensing, and CMB weak lensing allows robust constraints without including any information regarding $\tau_{\rm reio}$ (Boyle 2019; Brinckmann et al. 2019; Xu et al. 2021).

However, smaller uncertainties of the order of $\sigma(M_\nu) \simeq 10$ meV have been predicted only in combination with a tighter constraint on the optical depth at recombination $\sigma(\tau_{\rm reio}) \simeq 0.001$–$0.002$ (Yu et al. 2018; Brinckmann et al. 2019).

Using a three-tracer approach that combines clustering measurements from two next-generation large-scale structure surveys together with CMB-S4 measurements, we showed that if only linear scales are included, the 21 cm IM surveys outperform the photometric LSST survey.

The multitracer combination of CMB-S4 with IM delivers

$$\sigma\,(M_\nu) \simeq \begin{cases} 45\ \text{meV} & \text{SKAO-MID} \times \text{CMB-S4}\,, \\ 26\ \text{meV} & \text{PUMA} \times \text{CMB-S4}\,, \end{cases} \tag{32}$$

for $k_{\rm max} = 0.1\,h\,{\rm Mpc}^{-1}$, and when marginalizing over six standard cosmological parameters and over all nuisance parameters (27 for SKAO-MID and 57 for PUMA). These results are not sensitive to increasing $\ell_{\rm min}$ up to 20 since the extra constraining power comes from the cross-correlation between CMB lensing with IM.

When all three tracers are included in a multitracer analysis, the tightest uncertainties predicted are

$$\sigma(M_\nu) \simeq 12/11\ \text{meV}\ \ \text{SKAO-MID/PUMA} \times \text{LSST} \times \text{CMB-S4}\,. \tag{33}$$

Improved constraints in the linear regime can be obtained if we assume a prior on the reionization optical depth (see Table 3).

In Chen, Lee & Dvorkin (2021), the one-loop power spectrum (allowing an increase in $k_{\rm max}$) and the tree-level bispectrum are used to significantly improve constraints from the cross-correlation of LSST and CMB-S4 (see also Chudaykin & Ivanov 2019; Kamalinejad & Slepian 2020; Hahn & Villaescusa-Navarro 2021, for galaxy bispectrum constraints on M_ν). Here we have avoided the complexities of going beyond linear modelling, relying instead on the multitracer combination of the first-order power spectra of two large-scale structure surveys together with CMB.

ACKNOWLEDGEMENTS

MB acknowledges financial contribution from the contract Agenzia Spaziale Italiana (ASI)/Istituto Nazionale di Astrofisica (INAF) for the Euclid mission n.2018-23-HH.0. RM is supported by the South African Radio Astronomy Observatory (SARAO), National Research Foundation (grant no. 75415), and by the UK STFC consolidated grant ST/S000550/1.

DATA AVAILABILITY

The data underlying this article will be shared on reasonable request to the corresponding author.

REFERENCES

Allison R., Caucal P., Calabrese E., Dunkley J., Louis T., 2015, Phys. Rev. D., 92, 123535
Alonso D., Ferreira P. G., 2015, Phys. Rev. D, 92, 063525
Alonso D., Bull P., Ferreira P. G., Maartens R., Santos M., 2015, ApJ, 814, 145
Alonso D., Ferreira P. G., Jarvis M. J., Moodley K., 2017, Phys. Rev. D, 96, 043515
Archidiacono M., Hannestad S., Lesgourgues J., 2020, J. Cosmol. Astropart. Phys., 9, 21
Ballardini M., Maartens R., 2019, MNRAS, 485, 1339
Ballardini M., Matthewson W. L., Maartens R., 2019, MNRAS, 489, 1950
Ballardini M., Braglia M., Finelli F., Paoletti D., Starobinsky A. A., Umiltà C., 2020, J. Cosmol. Astropart. Phys., 10, 44
Bardeen J. M., Bond J., Kaiser N., Szalay A., 1986, ApJ, 304, 15
Bayer A. E., Banerjee A., Seljak U., 2021, preprint (arXiv:2108.04215)
Bermejo-Climent J. R., Ballardini M., Finelli F., Paoletti D., Maartens R., Rubiño Martín J. A., Valenziano L., 2021, Phys. Rev. D, 103, 103502
Bird S., Viel M., Haehnelt M. G., 2012, MNRAS, 420, 2551
BOSS Collaboration, 2017, MNRAS, 470, 2617
Boyle A., 2019, J. Cosmol. Astropart. Phys., 1904, 38
Brinckmann T., Hooper D. C., Archidiacono M., Lesgourgues J., Sprenger T., 2019, J. Cosmol. Astropart. Phys., 1901, 59
Bull P., Ferreira P. G., Patel P., Santos M. G., 2015, ApJ, 803, 21
Castorina E., Sefusatti E., Sheth R. K., Villaescusa-Navarro F., Viel M., 2014, J. Cosmol. Astropart. Phys., 2, 49
Challinor A., Lewis A., 2011, Phys. Rev. D, 84, 043516
Chen S.-F., Lee H., Dvorkin C., 2021, J. Cosmol. Astropart. Phys., 5, 30
Chiang C.-T., Hu W., Li Y., Loverde M., 2018, Phys. Rev. D, 97, 123526
Chiang C.-T., LoVerde M., Villaescusa-Navarro F., 2019, Phys. Rev. Lett., 122, 041302
Chudaykin A., Ivanov M. M., 2019, J. Cosmol. Astropart. Phys., 11, 34
CMB-S4 Collaboration, 2016, preprint (arXiv:1610.02743)
Coles P., 1993, MNRAS, 262, 1065
Cosmic Visions 21 cm Collaboration, 2018, preprint (arXiv:1810.09572)
Cunnington S., Wolz L., Pourtsidou A., Bacon D., 2019, MNRAS, 488, 5452
Di Valentino E., Gariazzo S., Mena O., 2021, Phys. Rev. D, 104, 083504
Durrer R., Jalilvand M., Kothari R., Maartens R., Montanari F., 2020, J. Cosmol. Astropart. Phys., 12, 3
Eisenstein D. J., Hu W., 1997, ApJ, 511, 5
Fonseca J., Camera S., Santos M., Maartens R., 2015, ApJ, 812, L22
Hahn C., Villaescusa-Navarro F., 2021, J. Cosmol. Astropart. Phys., 4, 29
Hall A. C., Challinor A., 2012, MNRAS, 425, 1170
Hannestad S., 2006, Ann. Rev. Nucl. Part. Sci., 56, 137
Hirata C. M., Seljak U., 2003, Phys. Rev. D, 68, 083002
Howlett C., Lewis A., Hall A., Challinor A., 2012, J. Cosmol. Astropart. Phys., 1204, 27
Hu W., Eisenstein D. J., 1998, ApJ, 498, 497
Hu W., Okamoto T., 2002, ApJ, 574, 566
Hu W., White M. J., 1997, Phys. Rev. D, 56, 596
Ivanov M. M., Simonović M., Zaldarriaga M., 2020, Phys. Rev. D, 101, 083504
Jolicoeur S., Maartens R., De Weerd E. M., Umeh O., Clarkson C., Camera S., 2021, J. Cosmol. Astropart. Phys., 6, 39
Kaiser N., 1984, ApJ, 284, L9
Kamalinejad F., Slepian Z., 2020, preprint (arXiv:2011.00899)
Knox L., 1995, Phys. Rev. D., 52, 4307
Lattanzi M., Gerbino M., 2018, Front. Phys., 5, 70
Lesgourgues J., Pastor S., 2006, Phys. Rep., 429, 307
Lesgourgues J., Pastor S., 2012, Adv. High Energy Phys., 2012, 608515
Lewis A., Challinor A., Lasenby A., 2000, ApJ, 538, 473
Liu A., Pritchard J. R., Allison R., Parsons A. R., Seljak U., Sherwin B. D., 2016, Phys. Rev. D, 93, 043013
LoVerde M., 2014, Phys. Rev. D, 90, 083530
LoVerde M., 2016, Phys. Rev. D., 93, 103526
LSST Dark Energy Science Collaboration, 2018, preprint (arXiv:1809.01669)
Ma Z.-M., Hu W., Huterer D., 2005, ApJ, 636, 21
Mann B., Peacock J., Heavens A., 1998, MNRAS, 293, 209
MeerKLASS Collaboration, 2017, preprint (arXiv:1709.06099)
Planck Collaboration I, 2020a, A&A, 641, A1
Planck Collaboration VI, 2020b, A&A, 641, A6
Planck Collaboration VIII, 2020c, A&A, 641, A8
PUMA Collaboration, 2019, BAAS, 51, 53
Raccanelli A., Verde L., Villaescusa-Navarro F., 2019, MNRAS, 483, 734
Roy Choudhury S., Hannestad S., 2020, J. Cosmol. Astropart. Phys., 7, 37
Sailer N., Castorina E., Ferraro S., White M., 2021, preprint (arXiv:2106.09713)
Schmittfull M., Seljak U., 2018, Phys. Rev. D, 97, 123540
Sekiguchi T., Takahashi T., 2021, Phys. Rev. D, 103, 083516
Seljak U., 2009, Phys. Rev. Lett., 102, 021302
Sherwin B. D., Schmittfull M., 2015, Phys. Rev. D, 92, 043005
SKA Collaboration, 2020, Publ. Astron. Soc. Aust., 37, e007
Smith K. M., Hanson D., LoVerde M., Hirata C. M., Zahn O., 2012, J. Cosmol. Astropart. Phys., 1206, 14
Sprenger T., Archidiacono M., Brinckmann T., Clesse S., Lesgourgues J., 2019, J. Cosmol. Astropart. Phys., 2, 47
Takahashi R., Sato M., Nishimichi T., Taruya A., Oguri M., 2012, ApJ, 761, 152
Tanidis K., Camera S., 2021, MNRAS, 502, 2952
Vagnozzi S., Giusarma E., Mena O., Freese K., Gerbino M., Ho S., Lattanzi M., 2017, Phys. Rev. D, 96, 123503
Vagnozzi S., Brinckmann T., Archidiacono M., Freese K., Gerbino M., Lesgourgues J., Sprenger T., 2018, J. Cosmol. Astropart. Phys., 9, 1
Villaescusa-Navarro F., Marulli F., Viel M., Branchini E., Castorina E., Sefusatti E., Saito S., 2014, J. Cosmol. Astropart. Phys., 3, 11
Villaescusa-Navarro F., Bull P., Viel M., 2015, ApJ, 814, 146
Witzemann A., Alonso D., Fonseca J., Santos M. G., 2019, MNRAS, 485, 5519
Wong Y. Y. Y., 2011, Ann. Rev. Nucl. Part. Sci., 61, 69
Xu W. L., DePorzio N., Muñoz J. B., Dvorkin C., 2021, Phys. Rev. D, 103, 023503
Yu B., Knight R. Z., Sherwin B. D., Ferraro S., Knox L., Schmittfull M., 2018, preprint (arXiv:1809.02120)

This paper has been typeset from a TEX/LATEX file prepared by the author.